The Journal of Experimental Biology 212, 1781-1793
Published by The Company of Biologists 2009
doi:10.1242/jeb.029918

Embryonic temperature affects muscle fibre recruitment in adult zebrafish: genome-wide changes in gene and microRNA expression associated with the transition from hyperplastic to hypertrophic growth phenotypes

Ian A. Johnston[1,*], Hung-Tai Lee[1], Daniel J. Macqueen[1], Karthikeyani Paranthaman[1], Cintia Kawashima[2], Attia Anwar[1], James R. Kinghorn[1] and Tamas Dalmay[2]

[1]School of Biology, University of St Andrews, St Andrews, Fife KY16 8LB, UK and [2]School of Biological Sciences, University of East Anglia, Norwich, Norfolk NR4 7TJ, UK

*Author for correspondence (e-mail: iaj@st-and.ac.uk)

Accepted 12 March 2009

SUMMARY

We investigated the effects of embryonic temperature (ET) treatments (22, 26 and 31°C) on the life-time recruitment of fast myotomal muscle fibres in zebrafish *Danio rerio* L. reared at 26/27°C from hatching. Fast muscle fibres were produced until 25 mm total length (TL) at 22°C ET, 28 mm TL at 26°C ET and 23 mm TL at 31°C ET. The final fibre number (FFN) showed an optimum at 26°C ET (3600) and was 19% and 14% higher than for the 22°C ET (3000) and 31°C ET (3100) treatments, respectively. Further growth to the maximum TL of ~48 mm only involved fibre hypertrophy. Microarray experiments were used to determine global changes in microRNA (miRNA) and mRNA expression associated with the transition from the hyperplasic myotube-producing phenotype (M^+, 10–12 mm TL) to the hypertrophic growth phenotype (M^-, 28–31 mm TL) in fish reared at 26–27°C over the whole life-cycle. The expression of miRNAs and mRNAs obtained from microarray experiments was validated by northern blotting and real-time qPCR in independent samples of fish with the M^+ and M^- phenotype. Fourteen down-regulated and 15 up-regulated miRNAs were identified in the M^- phenotype together with 34 down-regulated and 30 up-regulated mRNAs (>2-fold; $P<0.05$). The two most abundant categories of down-regulated genes in the M^- phenotype encoded contractile proteins (23.5%) and sarcomeric structural/cytoskeletal proteins (14.7%). In contrast, the most highly represented up-regulated transcripts in the M^- phenotype were energy metabolism (26.7%) and immune-related (20.0%) genes. The latter were mostly involved in cell–cell interactions and cytokine pathways and included β-2-microglobulin precursor (*b2m*), an orthologue of complement component 4, invariant chain-like protein 1 (*iclp*), CD9 antigen-like (*cd9l*), and tyrosine kinase, non-receptor (*tnk2*). Five myosin heavy chain genes that were down-regulated in the M^- phenotype formed part of a tandem repeat on chromosome 5 and were shown by *in situ* hybridisation to be specifically expressed in nascent myofibres. Seven up-regulated miRNAs in the M^- phenotype showed reciprocal expression with seven mRNA targets identified in miRBase Targets version 5 (http://microrna.sanger.ac.uk/targets/v5/), including asporin (aspn) which was the target for four miRNAs. Eleven down-regulated miRNAs in the M^- phenotype had predicted targets for seven up-regulated genes, including dre-miR-181c which had five predicted mRNA targets. These results provide evidence that miRNAs play a role in regulating the transition from the M^+ to the M^- phenotype and identify some of the genes and regulatory interactions involved.

Supplementary material available online at http://jeb.biologists.org/cgi/content/full/212/12/1781/DC1

Key words: *Danio rerio*, microRNA, developmental plasticity, temperature, muscle growth, muscle hyperplasia, gene expression, myosin heavy chains, β-2-microglobulin.

INTRODUCTION

In the myotomes of teleost fish, myotube production and the production of fast muscle fibres (hyperplasia) continues until around 40% of the maximum body length (Weatherley et al., 1988; Johnston et al., 2004). Once the final fibre number (FFN) is established, myotube formation is switched off and growth only involves nuclear accretion and an increase in fibre length and diameter (hypertrophy) (Weatherley et al., 1988; Johnston et al., 2004). Remarkably, in some species, such as the Atlantic salmon (*Salmo salar* L.), embryonic temperature treatment has been shown to have persistent effects on muscle fibre recruitment, affecting the FFN in adult stages (reviewed by Johnston, 2006). Little is known about changes in gene expression accompanying the transition between growth phenotypes in fish (Fernandes et al., 2005), and nothing about the pathways regulating muscle fibre number.

MicroRNAs (miRNAs) are an important class of 18–24 nucleotide non-coding RNAs that are repressive post-transcriptional regulators of gene expression (Bartel, 2004) involved in most if not all physiological processes, including stem cell differentiation, cell lineage specification, haematopoiesis, neurogenesis, myogenesis, immune responses, insulin secretion and cholesterol metabolism (reviewed by Williams, 2008). Computational studies suggest that around one-third of the protein-coding genes in the human (*Homo sapiens*) genome are subject to miRNA regulation (Lewis et al., 2005). miRNAs are derived from precursor transcripts containing hairpin structures. The ribonuclease III, Drosha, cleaves the primary transcript (pri-miRNA), releasing ~60–80 nucleotide precursor miRNA (pre-miRNA) hairpins (Lee et al., 2003). The pre-miRNA is transported to the cytoplasm by Exportin-5 and the endonuclease Dicer processes the stem–loop to a ~21 bp RNA duplex (Hutvagner and Zamore, 2002). Although the two strands of the duplex are

initially present in equal amounts, their accumulation is asymmetric at steady state, with the more abundant product referred to as the miRNA and the other stand as a miRNA* species (Okamura et al., 2008). The miRNA is preferentially incorporated into the RNA-induced silencing (RISC) complex. Recent studies indicate that more than 40% of miRNA* species are well conserved across *Drosophila* species, can associate with Argonaute proteins and also have regulatory activity, adding to the richness of miRNA regulation (Okamura et al., 2008).

miRNAs are thought to block translation because the RISC component Ago 2 precludes the binding of the transcription factor eIF4e to the 7-methylguanosine cap of the target mRNA (Kiriakidou et al., 2007). Animal miRNAs show imperfect base pairing to sequences within the 3′ untranslated region (UTR) of target mRNAs, although complementarity is higher for the so-called seed region (nucleotides 2–8 from the 5′ end) (Doench and Sharp, 2004). The 3′ UTRs of mRNAs form complex secondary and tertiary structures *in vivo*, influenced by the intracellular environment and unknown interactions with RNA transcripts and/or proteins, making it difficult to predict the single stranded regions that are accessible to miRNA binding (Zhao and Srivastava, 2007). In addition to their effects on inhibiting translation, miRNAs can affect the stability of mRNAs and mediate their degradation (Bagga et al., 2005). There is evidence that components of RISC, miRNAs and their targets are co-localised to cytoplasmic P-bodies which are thought to act as sites of programmed mRNA degradation (Chan and Slack, 2006). miRNAs may therefore have an important role in phenotypic transitions by removing mRNAs that have become inappropriate for the current physiological and/or ontological state.

There are a number of miRNAs that are strongly expressed in muscle, including miR-1, miR-133 and miR-206, which interact with evolutionarily conserved and well characterised transcriptional networks involved in regulating myogenesis (Rao et al., 2006). Experimentally verified targets for miR-1 include histone deacetylase 4 (HDAC4), which represses the transcription factor MEF2C and inhibits muscle differentiation (Lu et al., 2000). miR-206 was also stimulated by the master transcription factor myoD (Rosenberg et al., 2006), although it was shown that miR-206 is mainly induced by myf5 (Sweetman et al., 2008). Switching C2C12 myoblast cultures from media promoting proliferation to media inducing differentiation resulted in a marked up-regulation of miR-1, miR-133 and miR-206 (Chen et al., 2006). *In vivo*, functional overload leading to fibre hypertrophy in the mouse resulted in decreased expression of miR-1 and miR-133 (McCarthy and Esser, 2007). Not all the miRNAs involved in the regulation of myogenesis are specifically expressed in muscle. For example, the broadly expressed miR-181 targets Hox-A11, a repressor of myoD expression. Depletion of miR-181 in C2C12 cultures reduced myoD expression and inhibited the differentiation of myoblasts to myotubes (Naguibneva et al., 2006).

The first aim of this study was to determine the effect of embryonic temperature treatment on the life-time recruitment of fast muscle fibres in the zebrafish, a tractable model species with a sequenced genome. The second aim was to use microarrays to identify global changes in mRNA and miRNA expression associated with the transition from hyperplastic to hypertrophic muscle growth phenotypes. In order to identify putative regulatory networks, we then followed a similar approach to that of Tian and colleagues (Tian et al., 2008) involving examining the reciprocal expression of a miRNA and computationally predicted target within a defined physiological context. However, whereas Tian and colleagues matched changes in miRNA and protein expression we identified regulated mRNAs that were predicted targets for reciprocally expressed miRNAs.

MATERIALS AND METHODS

Fish

The F2 generation of a strain of zebrafish originally sourced from a Singapore fish farm were used in all experiments. Broodstock comprised 15 females and 8 males maintained in a freshwater re-circulation system at 26–27°C (12 h dark:12 h light photoperiod). Fish were fed twice daily with bloodworm to bring them into peak breeding condition. The 1–4 cell stage embryos from a minimum of three spawnings (~600–1000 per spawning) were incubated at embryonic temperature treatments of 22, 26 or 31°C (±0.5°C). After hatching, the larvae were transferred to duplicate tanks maintained at a common temperature of 26–27°C (12 h light:12 h dark). Fish were initially fed 80–200 μm size fry food (ZM, Winchester, UK) and later proprietary flakes supplemented with bloodworm. Zebrafish were killed by an overdose of MS222 and pithing. Morphological measurements were made at each experimental temperature whereas expression studies were only carried out on fish reared at 26°C throughout the whole life-cycle.

Characterisation of fast muscle phenotypes

Frozen sections (7–10 μm thick) of the trunk were prepared at 0.6 total length (TL) and stained with Meyer's haematoxylin, succinic dehydrogenase and the S58 antibody to slow muscle myosin in order to differentiate slow, intermediate and fast muscle fibre types as previously described (Johnston et al., 2004). Sections were photographed and the total cross-sectional area of fast muscle was digitised (Sigma Scan Pro 5, SPSS, Chicago, IL, USA). The cross-sectional areas of individual fast fibres were measured in a half-myotomal cross-section. For larvae and juveniles (<12 mm TL) all the fibres were digitised whereas for larger fish 8–10 square fields of 0.028 mm^2, containing 800–1000 fibres, were measured. Fibre number was estimated as previously described (Johnston et al., 1999). Two methods were used to estimate the FFN in adult fish. A direct estimate was obtained from the fibre number in fish with <0.2% of fibres in the smallest size class, 7–10 μm diameter. In addition, in an exploratory analysis three classes of asymptotic curves (logistic, von Bertalanfyy and Gompertz) were fitted to the entire data set for each embryonic temperature treatment. Models were fitted with a weighted variance function using the nlme library in R (see Pinheiro and Bates, 2000). Akaike's Information Criteria identified the Gompertz curve as the best model (Eqn 1):

$$FN_i = \alpha_j \exp[-\exp(\beta - \gamma \times TL_{ij})] , \quad (1)$$

where FN, is fibre number; i and j index the ith datum within treatment group j; α_j, β and γ are parameters to be estimated; α_j represents the asymptote, γ describes the rate at which the curve ascends and β is a constant.

Expression analysis

Two stages were used for expression studies based on morphological measurements: (1) adults that were still actively recruiting myotubes (M^+ stage) and (2) adults that had ceased myotube production (M^- stage). The fish from M^+ and M^- stages were 10–12 mm TL and 28–31 mm TL, respectively. For each RNA extraction for microarray experiments, the pooled dorsal epaxial fast muscle from 10 individuals was used for the M^+ stage and from two individuals for the M^- stage. Total RNA was isolated using the mirVana miRNA isolation kit (Ambion, Austin, TX, USA) and quantified using a

Nanodrop spectrophotometer (Thermo Fisher Scientific, Loughborough, UK).

miRNA microarrays

The differential expression of miRNAs between M^+ and M^- phenotypes was studied using a microarray with probes designed from the miRBase sequence database version 8.2 (Sanger Institute, Cambridge, UK; http://www.microRNA.sanger.ac.uk/sequences). Total RNA (10 µg) was analysed by LC Sciences (Houston, TX, USA) microRNA microarray service (http://www.lcsciences.com). The samples were enriched for small RNAs and labelled with fluorescent dyes: Cy3 for M^+ and Cy5 for M^- phenotypes. A pair of labelled samples (six replicates) was hybridised to µParaFlo^R microfluidic chips. Each chip includes multiple redundant regions for each miRNA. Multiple control probes were included in each chip. The stringency was estimated from the intensity ratio (>30) of perfect match and single-based match detection probes. The data were filtered and $\log_2$ transformed and significant differences (probability values) between M^+ and M^- phenotypes calculated using paired *t*-tests (Minitab, State College, PA, USA). The European Bioinformatics Institute accession number for this experiment is E-TABM-526.

Northern blotting

As a first step to validating targets and to confirm the microarray data, we performed northern blot analysis using total RNA from independent samples comprising three individuals per phenotype. Approximately 30 µg of total RNA for each sample was separated in a denaturing 15% (m/v) polyacrylamide gel by electrophoresis. RNA was transferred to zeta probe membranes (BioRad, Hemel Hempstead, UK) using a semi-dry electro-blotting unit (Fisher Brand, Loughborough, UK) and membranes were UV cross-linked. The selected miRNA probe sequences (supplementary material Table S1) were cross-checked with the sequences listed in the miRNA registry (http://www.sanger.ac.uk/software/Rfam/mirna/). Oligonucleotides of the reverse complement to the mature miRNA were used as probes. Probes (10 µmol l^{-1}) were prepared by T4 polynucleotide kinase labelling of antisense oligonucleotides with γ^{32}P dATP (1.5 MBq). Pre-hybridisations and hybridisations were carried out using Ultra-Hyb oligo hybridisation buffer (Ambion) at 37°C and the blots were washed twice with 0.2× SSC/0.1% (w/v) SDS at 37°C. The membranes were exposed to a phosphor storage screen, incubated at room temperature for 4–5 days and analysed using a Personal Molecular Imager FX (BioRad).

Dot blots of control probes corresponding to specific miRNAs were used to verify transfer and hybridisation, using primers with identical sequences to mature miRNAs. RNA oligonucleotides 19 and 24 nucleotides long were used as size markers. Equal loading of the gels was confirmed by re-probing the filters with a ^{32}P-labelled U6 RNA probe. Filters were stripped and re-probed up to 5 times. Loss of the probe was confirmed by phosphorimaging of the membrane before re-probing. Quantitative analysis of radiolabelled probes hybridising to blots was performed by auto-radiography using an Instant Imager (Canberra Packard, Meriden, CT, USA). Signals appearing on the northern blots were normalised to the corresponding U6 signal. Variations in the amount of total RNA present on the blot were calculated using U6 and used to adjust the final radioactive signals obtained to values per microgram of total RNA from the hybridisation. Statistical analysis was performed using StatView 4.01 software (Abacus Concepts, Berkeley, CA, USA), using ANOVA followed by Scheffe's *F* post-analyses of significance.

Genome microarrays

Hybridisations were performed using eight RNA extractions per phenotype and microarray experiments were performed using a two-colour-based gene expression system at an Agilent (Palo Alto, CA, USA) certified microarray service provider (University Health Network, Toronto, ON, Canada). Arrays were scanned using Gene pix 4000A/B scanners. Evaluation of data for microarray analysis was performed using Gene Spring software (Agilent Technologies, Mississauga, ON, Canada). Signal intensities reflected overall expression level and a detection confidence score. Signals were $\log_2$ transformed and those that were at or below background level were discarded. Genes were filtered based both on the fold-change of ±2 and on confidence with a *P*-value ≤0.05. The differentially expressed genes were then clustered using the gene tree function with a Pearson correlation and average linkage. Fold-change in expression was calculated from the average signal intensity of each group and mRNAs with a fold-change ≥2 were selected for further consideration. The European Bioinformatics Institute accession number for this experiment is E-TABM-552.

Validation of microarray results by quantitative real-time PCR (qPCR)

The expression patterns of genes differentially expressed between M^+ and M^- stages in the microarray experiment were examined by qPCR. A set of fast muscle RNA samples independent from those in the microarray was used. For M^+ stages, dissections pooled from three zebrafish of 9–12 mm TL were used for each of five samples. For M^- stages, fast muscles of five individual zebrafish of 28–34 mm TL were used. Total RNA was obtained using a standard phenol:chloroform extraction method. RNA concentration and contamination carry-over were analysed using a NanoDropTM 1000 spectrophotometer (Thermo Scientific). All RNA had 260 nm:280 nm absorbance ratios between 1.9 and 2.3 and 260 nm:230 nm absorbance ratios of >2.2. The integrity of RNA was confirmed by analysing ~1 µg of RNA by agarose gel electrophoresis and each sample had clear 28S and 18S ribosomal RNA bands with no visible RNA degradation. cDNA synthesis with 850 ng of total RNA was carried out using the QuantiTect reverse transcription kit (Qiagen, Hilden, Germany) following the manufacturer's instructions and including a genomic DNA removal step. To reduce carried-over 'poisons' that might reduce qPCR efficiency, cDNA was diluted 100 times in nuclease-free water. The expression of 16 candidate genes was examined using the primers listed in supplementary material Table S2. Primers were designed to distinguish between all potential paralogues that could be identified in Ensembl (release 51; WTSI/EBI, Cambridge, UK) and NCBI zebrafish databases and so that at least one in each pair spanned an exon boundary. In three cases, this was not possible due to the limited regions available to distinguish certain highly homologous gene paralogues, although these primers were still positioned within different exons. A 4 µl sample of each cDNA was used as a template for qPCR, using 10 µl Brilliant SYBR Green QPCR master mix (Stratagene) and a Mx30005P qPCR thermocycler (Stratagene, La Jolla, CA, USA), in 20 µl reactions, performed in duplicate and containing 200 nmol of primer. Cycling parameters were as follows: one cycle of 15 min at 95°C, 40 cycles of 30 s at 95°C, 30 s at 60°C and 30 s at 72°C, followed by a DNA dissociation analysis. Sybergreen fluorescence was recorded during the extension phase of cycling. Each qPCR plate contained all sample cDNAs to avoid plate-to-plate heterogeneity. To estimate the amplification efficiency of each primer set, a cDNA dilution series was created from a pool of all cDNAs. Raw data were analysed

using Mx30005P qPCR software (Stratagene) and the threshold fluorescence of dRn values was adjusted to be in the exponential phase of amplification. Cycle threshold values of samples and the dilution series were manually exported into REST 2008 (Pfaffl et al., 2002) (downloaded from http://www.gene-quantification.de/rest-2008.html), which was used to calculate reaction efficiencies and relative expression levels of M^+ and M^- samples, normalised to the expression of two housekeeping genes (β-actin and *rpl13*) that were stably expressed across samples. To assess statistical differences in relative expression values, a non-parametric randomisation test was performed, using 5000 bootstrap replicates to resample the expression differences.

In situ hybridisation of a *myhz1* RNA probe to M^+ and M^- muscle

Briefly, a standard RT-PCR reaction was used with primers specific to *myhz1(2)* (supplementary material Table S2), to amplify a double-stranded cDNA product that was ligated into pCR4-TOPO T/A vector (Invitrogen, Paisley, UK) and transformed into competent *Escherichia coli* (Invitrogen). Cloned products were sequenced using T3/T7 primers to confirm the expected sequence and determine strand orientation. This demonstrated that the primers amplified the most divergent region of *myhz(2)* (the extreme 3′ UTR) which shares no more than 85% sequence identity with other *myhz* genes on the tandem (not shown). T3 and T7 RNA polymerases (Roche Diagnostics, Burgess Hill, West Sussex, UK) were used to synthesise RNA probes in sense and antisense directions with concurrent incorporation of digoxigenin (Roche) following the manufacturer's instructions. *In situ* hybridisation of probes to small bundles of fast muscle stripped from the epaxial myotomes of M^+ and M^- zebrafish was performed using a modified standard protocol (Thisse and Thisse, 2008). Hybridised probes were detected with an alkaline phosphatase-conjugated anti-digoxigenin antibody (Roche) using NBT/BCIP (Roche). Cryosectioning of muscle bundles was performed using a cryostat (Leica Microsystems, CM1850, Nussloch, Germany) after first freezing tissues in isopentane cooled to –159°C with liquid N_2.

miRNA target prediction

Computationally predicted targets associated with the significantly differentially expressed miRNAs were obtained from the miRBase Targets Version 5 database (http://microrna.sanger.ac.uk/targets/v5/). Down-regulated miRNAs were matched with the predicted up-regulated mRNA targets and *vice versa*. The miRBase Targets database uses the miRanda algorithm to identify potential binding sites for a given miRNA in genomic sequences. In the current version of the program, alignments require no more than one base in the 'seed region' at the 5′ end of the miRNA to be non-complementary for the target to be discarded. Targets selected in this manner are further screened for thermodynamic stability of RNA folding and for conservation of alignment in the 3′ UTR of orthologous genes in at least two species (see http://microrna.sanger.ac.uk/targets/v5/info.html for further details).

Phylogenetic analysis of vertebrate fast skeletal muscle myosin heavy chain proteins

The evolutionary relationships of fast muscle myosin heavy chain (MyHC) genes orientated in tandem in several vertebrate genomes were reconstructed using phylogenetic analysis. Full-length amino acid sequences of 28 MyHC genes were obtained from release 51 Ensembl genome databases of zebrafish, stickleback (*Gasterosteus aculeatus*), tiger pufferfish (*Takifugu rubripes*), green-spotted pufferfish (*Tetraodon nigroviridis*) and human. Sequences were aligned using promals (Pei and Grishin, 2007) followed by manual alignment quality checking and removal of indels. The sequence alignment is available on request to I.A.J. Maximum likelihood was performed with Phyml (Guindon and Gascueal, 2003), using the LG model, with concurrent estimation of the γ-distribution of among-site rate variation, the number of invariable sites and employing 1000 bootstrap replicates. Neighbour joining (NJ) and maximum parsimony (MP) analyses were performed using Mega 4.0 (Tamura et al., 2007), resampling the data with 1000 bootstrap iterations as a measure of branch confidence.

RESULTS

Muscle fibre formation

The relationships between the number of fast muscle fibres per myotomal cross-section and fish TL (mm) for different embryonic temperature treatments are shown in Fig. 1A. Two patterns of post-embryonic muscle fibre production were sequentially observed in zebrafish as evidenced by the spatial distribution of fibre diameters.

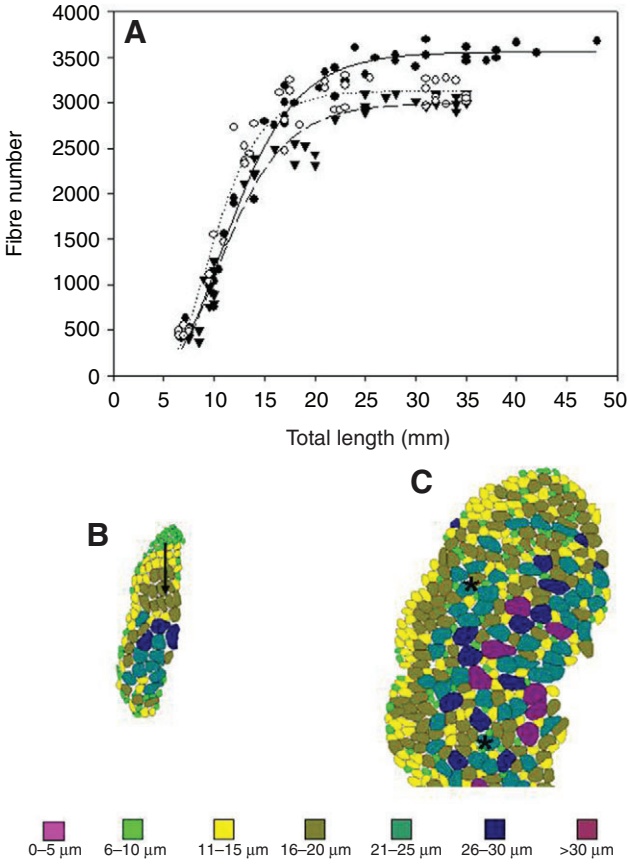

Fig. 1. (A) The relationship between fish total length (TL, mm) and the number of fast muscle fibres per myotomal cross-section at 0.6 TL for embryonic temperature treatments of 22°C (*N*=41, filled triangles), 26°C (*N*=44, filled circles) and 31°C (*N*=46, open circles). Gompertz curves were fitted to the data (see text): 22°C, dashed line, Rsqr=0.97; 26°C, solid line, Rsqr=0.98; 31°C, dotted line, Rsqr=0.97). (B) Camera lucida drawing of the fast muscle fibres in a fish of 7.5 mm TL from the 22°C embryonic treatment, colour coded according to fibre diameter size class. The arrow illustrates layers of increasing fibre diameter (stratified hyperplasia). (C) Camera lucida drawing of the fast muscle fibres in a fish of 10 mm TL from the 31°C embryonic treatment, colour coded according to fibre diameter size class. The asterisks mark fibres surrounded by daughter fibres, characteristic of mosaic hyperplasia.

Stratified hyperplasia involves the production of myotubes in discrete zones, resulting in layers of fibres of increasing diameter with increasing distance from the site(s) of fibre production (arrow in Fig. 1B). In the smallest fish, ~7–8 mm TL, stratified hyperplasia was the only mechanism of fibre expansion apparent, except in a few individuals from the 31°C ET treatment. In larger fish, mosaic hyperplasia was the predominant means of expansion of fibre number, with fibres of the smallest size class occurring on the surface of existing muscle fibres throughout all regions of the myotomal cross-section (illustrated by asterisks in Fig. 1C). The final number of muscle fibres (FFN) produced was estimated from the asymptote of a Gompertz curve fitted to values of fibre number and TL (Table 1). Values of FFN obtained from the Gompertz model were in good agreement with average values calculated from fish that had no fibres in the smallest size class (7–10 μm; Table 1). ET treatment resulted in significant differences in FFN ($P<0.01$). From the model, FFN was 18.8% higher at 26°C than at 22°C ($P<0.01$) and 13.7% higher at 26°C than at 31°C ($P<0.05$). The fish length at which the recruitment of fast muscle fibres stopped, estimated from the Gompertz model, was 23.0 mm at 31°C increasing to 27.8 mm at 22°C and 29.8 mm at 26°C (Table 1). Thus, ET treatment also had a significant effect on the body length at which the transition between M^+ and M^- phenotypes occurred. In contrast, the relationship between the cross-sectional area of fast myotomal muscle and TL was similar for all ET treatments (not shown).

miRNA expression

One-hundred and sixty-eight miRNAs were expressed in the fast myotomal muscle of adult zebrafish reared at 26–27°C over the whole life-cycle out of 219 miRNAs on the microarray, although only 75 were consistently expressed in all individuals. We assessed the relative expression of miRNAs on the basis of their background-subtracted and normalised fluorescence intensity signals and classified them as high (20,000–55,000 units), moderate (10,000–19,999 units) or low (2000–9900) abundance. The most abundant miRNAs were miR-1, let-7a, let-7c, let-7f, miR-17a, miR20a,b, miR-126, miR-133c, miR-181a, miR-203b, miR-206, miR-214 and miR-738. As absolute expression is influenced by variation in probe concentration and the efficiency of printing pins, this result should be treated with caution. We identified 14 miRNAs that were up-regulated (Fig. 2) and 15 miRNAs that were down-regulated in the M^- phenotype in 6/6 individuals (Fig. 3). The expression of a selection of the differentially regulated miRNAs was successfully validated by northern blotting (supplementary material Table S1; Fig. 4). The signal intensity of northerns was quantified and normalised to U6, and found to correlate well with the microarray data (Fig. 4). Five members of the dre-let-7 family of miRNA (let-7b, e, g, h, j) were consistently up-regulated in the M^- phenotype (Fig. 2). Three members of the dre-miR-19 family (miR-19b, c, d) and two members of the dre-miR-130 family (miR-130b, c) were significantly down-regulated in the M^- phenotype (Fig. 3). The most down-regulated miRNA in the M^- phenotype by 47/34-fold (microarray/northerns) was dre-miR-9*, the expression of which was relatively low (Figs 3 and 4).

mRNA expression

A whole genome zebrafish array was used to identify genes differentially expressed by at least 2-fold between 8/8 M^+ and M^- samples with a significance level of $P<0.05$. The identity of the genes was confirmed by blasting the probe sequence on the array against the zebrafish genome assembly version 7 (Zv7; http://ensembl.genomics.org.cn/Danio_rerio/index.html) and non-redundant nucleotide and EST databases (http://blast.ncbi.nlm.nih.gov/). When closely related putative paralogues were identified for sequences on the array, the identity shared by probe sequences and corresponding regions in their paralogues was calculated to check for potential spurious cross-hybridisation artifacts. Following this analysis there were 34 down-regulated genes (Table 2) and 30 up-regulated genes (Table 3) in the M^- phenotype (Fig. 5). The three most down-regulated genes (by 10- to 20-fold) in the M^- phenotype together with the sixth (by ~9-fold) and eighth (by 7-fold) most down-regulated genes corresponded to MyHC genes (Table 2). These MyHC genes were part of a tandem repeat on chromosome 5 (Fig. 6). Expression of all five down-regulated MyHC genes was validated by qPCR, using highly specific primers and fold down-regulation was generally even greater than that observed on the microarray (Fig. 6). The final member of the cluster not detected by the microarray analysis was shown by qPCR to be significantly up-regulated in the M^- phenotype (Fig. 6). The spatial expression of one of the MyHC genes [*myhz1(2)*] was investigated by *in situ* hybridisation. *myhz1(2)* was highly expressed in nascent muscle fibres, but not in larger diameter fibres (Fig. 6). The discovery of these MyHC genes using the approach adopted is highly encouraging because the M^- phenotype was defined in terms of the absence of myotubes and the smallest size class of muscle fibre.

The genomes of several other vertebrates have similar tandems of fast skeletal muscle MyHC genes [e.g. stickleback (*Gasterosteus aculeatus*), human, Fig. 6; medaka (*Oryzias latipes*) (Liang et al., 2007)]. A maximum likelihood phylogenetic analysis was performed for complete amino acid sequences of these genes for zebrafish, stickleback and human, within a framework containing in total 13 human MyHC genes (Fig. 6). To test the sensitivity of the tree topology to the reconstruction method, neighbour joining and maximum parsimony analyses were also performed on the same data, producing highly comparable well-supported trees (not shown). All the included vertebrate fast skeletal MyHC sequences found in tandems branched as a clade internal to other MyHC types, many of which are conserved in both teleosts and mammals, and including

Table 1. Determination of the final number of fast myotomal muscle fibres (FNN) in adult zebrafish (*Danio rerio* L.) subject to embryonic temperature treatments of 22, 26 and 31°C

Embryonic temperature (°C)	FFN		TL at which FFN is reached (mm)	
	Model	Observation	Model	Observation
22	2995±43	3009±28 (N=15)	27.8	25.0
26	3558±38	3559±35 (N=15)*	29.8	28.0
31	3130±43	3081±35 (N=18)	23.0	23.0

The relationship between fibre number and total length (TL) was fitted with a Gompertz model enabling FFN (the asymptote; means ± s.e.m.) and the TL at which FFN was reached to be calculated (model). These values were compared with estimates based on the longest fish containing no fast muscle fibres less than 10 μm diameter (observation).

Asterisk indicates a significant difference analysed by ANOVA and Fisher's test ($P<0.01$).

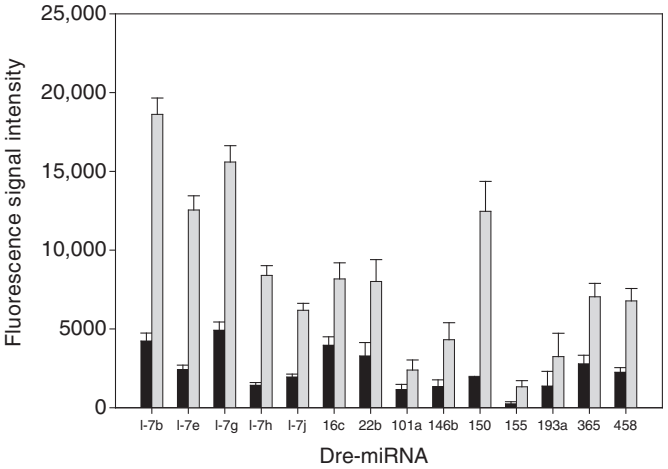

Fig. 2. The signal intensity of microRNAs on the arrays that were up-regulated in the M⁻ phenotype from microarray experiments. Solid and open bars represent background-subtracted and normalised fluorescence signals in the myotube (+) (M^+) and myotube (–) (M^-) muscle growth phenotypes of zebrafish, respectively. Values represent means ± s.e.m., six fish per phenotype. Dre-miRNA, *Danio rerio* microRNA; l-7, let-7.

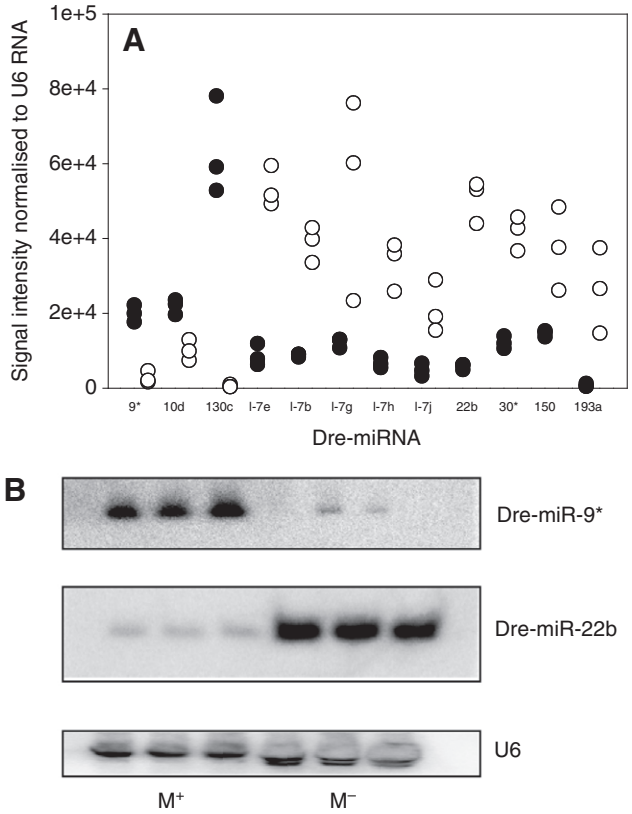

Fig. 4. (A) Validation of selected miRNAs by northern blotting (see text for details). Filled and open circles represent signals in the M^+ and M^- muscle growth phenotypes, respectively. (B) Representative northern blots of RNA from M^+ and M^- phenotypes with a U6 RNA loading control. The sequence of primers used is shown in supplementary material Table S1.

cardiac and other non-fast skeletal muscle isoforms (Fig. 6). Zebrafish and stickleback fast skeletal MyHC cluster sequences branched internally to *myh13* of the human cluster. Therefore, it is possible that the tandem zebrafish/stickleback fast skeletal MyHC genes and their single orthologues in pufferfish are actually co-orthologues of *myh13* and that other human MyHC genes on the tandem were derived independently. Further, zebrafish and stickleback clusters form separate clades (Fig. 6), suggesting that these tandem arrangements were independently derived after the speciation event separating these lineages.

The relatively small numbers of differentially expressed genes were classified manually according to their function based on a search of the literature primarily using the PubMed, GoogleScholar, iHop (http://www.ihop-net.org/) and Kegg (http://www.genome.jp/kegg/) databases. The most abundant categories of down-regulated genes in the M⁻ phenotype were contractile proteins (23.5%) and sarcomeric structural/cytoskeletal proteins (14.7%, Table 2; Fig. 5). The next most abundant category of down-regulated genes in the M⁻ phenotype was involved with either tyrosine metabolism or amino acid transport. Two genes encoding transcription factors were significantly down-regulated in the M⁻ phenotype on the array, the myogenic regulatory factor *myf5* and *sox11a* (Table 2). Cystathionine γ-lyase (*cth*), which catalyses the production of gaseous H_2S from cysteine and functions as a neuromodulator and physiological vasodilator involved in the regulation of blood pressure (Yang et al., 2008), was down-regulated 3.2-fold in the M⁻ phenotype (Table 2). There were two genes significantly down-regulated in the M⁻ phenotype that were involved in tyrosine metabolism (an orthologue of 4-hydroxy-phenyl pyruvate dioxygenase and fumarylacetoacetate hydrolase, *fah*) and melanin biosynthesis (tyrosine-related protein 1b, *tyrp1b*), perhaps reflecting some inadvertent contamination with pigment cells in the M^+ phenotype samples.

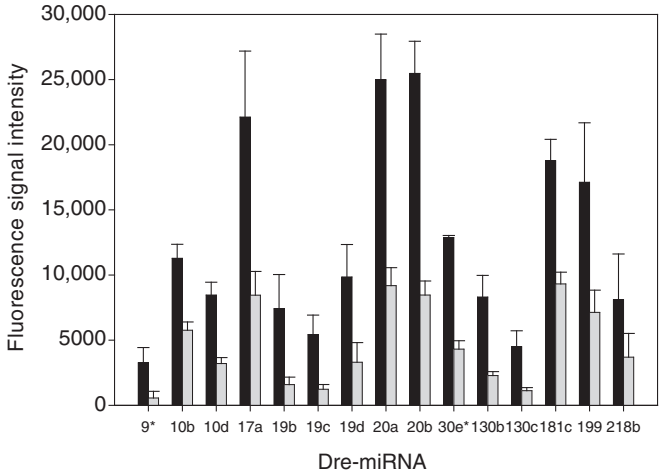

Fig. 3. The signal intensity of miRNAs on the arrays that were down-regulated in the M⁻ phenotype from microarray experiments. Solid and open bars represent background-subtracted and normalised fluorescence signals in the M^+ and M⁻ muscle growth phenotypes of zebrafish, respectively. Values represent means ± s.e.m., six fish per phenotype.

The significantly up-regulated genes in the M⁻ phenotype showed a very different profile with only contractile proteins and energy metabolism genes represented in the functional categories observed for the down-regulated genes (Fig. 5). *pvalb4*, which is a member of the parvalbumin gene family that code for sarcoplasmic Ca^{2+} binding proteins involved in muscle relaxation (Jiang et al., 1996), was up-regulated 8.3-fold on the microarrays (Table 3) and 16.9-fold by qPCR (Table 4). Immune-related genes related to cell–cell interactions and cytokine pathways comprised around 15% of the

up-regulated genes and included β-2-microglobulin precursor (*b2m*, 7.3-fold on array and 5.1-fold by qPCR), CD9 antigen-like (*cd9l*, 2.6-fold on array and 2.4-fold by qPCR), invariant chain-like protein 1 (*iclp1*) and tyrosine kinase, non-receptor 2 (*tnk2*, Table 3). Enolase 3 (eno3), a myoblast-specific enhancer was up-regulated 2.2-fold on the array and hypoxia-inducible factor 1, α-subunit inhibitor (*hif1an*) was up-regulated 2.8-fold on the array and 4.2-fold by qPCR (Tables 3 and 4). This latter protein functions as part of an oxygen-sensing system in muscle and under normoxic conditions hydroxylation of the C-terminal transactivation domain of HIF-1α by hif1an represses its transcription (Semenza, 1999). Two components of G-protein signalling were significantly up-regulated

Table 2. Genes that were consistently down-regulated 2-fold or more at the $P<0.05$ level in the M^- relative to the M^+ phenotype of zebrafish fast skeletal muscle

	ZFIN gene symbol and description		Fold down-regulation mRNA (mean ± s.e.m., $N=8$)	Predicted target match with up-regulated miRNA	Fold up-regulation miRNA (mean ± s.e.m., $N=6$)
1	*myhz1*	Myosin heavy chain[1]	22.1±2.0	0	–
2	*myhz1*	Myosin heavy chain[1]	15.6±0.7	0	–
3	*myhz1*	Myosin heavy chain[1]	11.1±0.6	0	–
4	*tnni 2*	Troponin I type 2 fast skeletal	11.0±1.6	0	–
5	*ptgds*	Prostaglandin D2 synthase	9.5±1.6	0	–
6	*myhz2*	Myosin heavy chain[1]	8.7±0.5	0	–
7	*tmsb*	Thymosin β	7.7±1.5	0	–
8	*A2BGX8_DANRE*	Myosin heavy chain[1,2]	7.3±0.9	0	–
9	*zgc:92456*	Orthologue 4-hydroxy-phenyl pyruvate dioxygenase	6.5±1.3	0	–
10	*tyrp1b*	Tyrosine-related protein 1	6.3±1.1	0	–
11	*zgc:114184*	Orthologue of troponin-T isoform	5.4±1.4	0	–
12	*fah*	Fumarylacetoacetate hydrolase	4.7±1.2	dre-miR-146b dre-miR-193a dre-miR-146b	3.5±0.5 5.2±0.9 3.5±0.5
13	*zgc:153151*	Similar to solute carrier family 7 member 8	4.4±0.7	0	–
14	*zgc:112098*	Orthologue of actin (α-sarcomeric 2)	4.3±0.2	0	–
15	*sox11a*	SRY-box containing gene 11a	4.1±1.1	0	–
16	*myf5*	Myogenic regulatory factor	4.0±0.5	0	–
17	*fzd8a*	Frizzled homologue 8a	4.0±0.6	dre-miR-365	2.7±0.4
18	*zgc:113456*	Orthologue of fibromodulin precursor (collagen-binding 59 kDa protein)	3.8±0.7	0	–
19	*aspn*	Asporin (LRR class 1)	3.7±0.4	dre-let-7e dre-miR-155 dre-miR-193a dre-miR-365	5.3±1.5 6.9±1.8 5.2±0.9 2.7±0.4
20	*cox6a1*	Cytochrome *c* oxidase subunit VIa polypeptide 1	3.5±0.4	dre-let-7e	1.9±0.1
21	*slc38a3*	Solute carrier family 38, member 3	3.5±0.4	0	–
22.	*zgc:13651*	Orthologue 60S ribosomal protein L22	3.4±0.5	0	–
23	*cth*	Cystathionine γ-lyase	3.2±0.3	0	–
24	*hhatl*	Hedgehog acyltransferase-like, a	3.1±0.5	0	–
25	*zgc:136609*	Hypothetical protein LOC 568616 SET and MYND domain-containing transcript	3.0±0.5	dre-let-7j	3.1±0.4
26	*fkbp1b*	FK506 binding protein 1b	2.8±0.4	dre-miR-365	5.2±0.9
27	*myca*	c-Myc oncoprotein	2.8±0.2	0	–
28	*atp1b3a*	Na^+,K^+-transporting β3a polypeptide	2.6±0.4	0	–
29	*LUC7L2*	Putative RNA binding protein Lu7-like	2.5±0.2	dre-miR-30e*	2.8±0.5
30	*zgc:92347*	Orthologue of myozenin-1 (calsarcin–calcineurine binding protein)	2.3±0.2	0	–
31	*psma5*	Proteasome subunit, α-type 5	2.3±0.3	0	–
32	*pdcl3*	Phosphoducin-like 3	2.2±0.1	0	–
33	*ctnna2*	Novel protein similar to human catenin (cadherins-associated protein α)		0	–
34	*ppia*	2-Peptidyl prolylisomerase A	2.0±0.2	0	–

M^- and M^+, myotube minus and plus phenotype, respectively.

Predicted target matches with upregulated miRNAs at the $P<0.05$ level from miRBase Targets Version 5 are shown (http://microrna.sanger.ac.uk/targets/v5/).

[1]Myosin heavy chain tandem repeat on chromosome 5: Chr5 23.978.407–23.989.519 (6, first in cluster); Chr5 23.993.774–24.005.897 (–, second in cluster); Chr5 24.019.329–24.09.268 (8, third in cluster); Chr5 24.033.98124.045.796 (3, fourth in cluster); Chr5 24.052.882–24.063.763 (1, fifth in cluster); Chr5 24.070.649–24.080.528 (2, sixth in cluster).

[2]Uni Prot KB/Tr EMBL.

in the M$^-$ phenotype, a regulator of G protein signalling 5 (*zgc:64006*) and ADP-ribosylation factor-like 6 interacting protein 1 (Tables 3 and 4).

Predicted mRNA targets of differentially expressed miRNAs

Seven of the down-regulated genes (20.5%) in the M$^-$ phenotype were predicted targets for significantly up-regulated miRNAs (Table 2). Two of these genes were predicted targets for miRNAs (three miRNAs for *fah* and four miRNAs for *aspn*; Table 2). Dre-miR365 was predicted to target three mRNAs (*fzd8a* which is a WNT inhibitor, *aspn* and *fkbp1b*; Table 2). Seven of the up-regulated genes in the M$^-$ phenotype were predicted targets for significantly down-regulated miRNAs (Table 3). Those mRNAs predicted to be targets for more than two miRNAs were *pvalb4* with four, glyceraldehyde 3-phosphate dehydrogenase (*gapdh*) with four, and regulator of G-protein signalling (*zgc:64006*) with three (Table 3). Dre-miR-181c was predicted to bind to the 3′ UTR of *pvalb4*, *gapdh*, *cd9l*, *zgc:64006* and *slc25a4* (Table 3).

DISCUSSION

Muscle growth phenotypes in zebrafish

Traditionally the expansion of muscle fibre number in teleosts has been described in morphological terms as the formation of myotubes at discrete germinal zones (stratified hyperplasia) or myotube

Table 3. Genes that were consistently upregulated by 2-fold or more at the $P<0.05$ level in the M$^-$ relative to the M$^+$ phenotype of zebrafish fast skeletal muscle

	ZFIN gene symbol	and description	Fold up-regulation mRNA (mean ± s.e.m., $N=8$)	Predicted target match with downregulated miRNA	Fold down-regulation miRNA (mean ± s.e.m., $N=6$)
1	*pvalb4*	Parvalbumin isoform 1c	8.3±1.0	dre-miR-17a	2.8±0.7
				dre-miR-20a	2.8±0.1
				dre-miR-20b	3.2±0.3
				dre-miR-181c	2.0±0.1
2	*b2m*	β-2-Microglobulin precursor	7.3±1.5	0	–
3	*zgc:56085*	Creatine kinase, sarcomeric mitochondrial precursor	4.8±0.5	0	–
4	*zgc:92069*	Protein phosphatase 1 regulatory subunit 3C (PPP1R3C)	3.8±0.6	0	–
5	*gapdh*	Glyceraldehyde 3-phosphate dehydrogenase	3.4±0.4	dre-miR-19b	11.0±4.4
				dre-miR-19c	6.3±1.8
				dre-miR-19d	11.2±1.7
				dre-miR-181c	2.0±0.1
6	*none*	Unannotated gene LOC794635 orthologue complement component 4	2.8±0.7	0	–
7	*hif1an*	Hypoxia-inducible factor 1, α-subunit inhibitor	2.8±0.3	0	–
8	*ckmb*	Creatine kinase, muscle b	2.8±0.4	NI	–
9	*zgc:91930*	Adenylate kinase isoenzyme 1	2.7±0.4	0	–
10	*ldha*	Lactate dehydrogenase A	2.6±0.4	0	–
11	*iclp1*	Invariant chain-like protein chain 1	2.6±0.4	0	–
12	*cd9l*	CD9 antigen-like	2.6±0.3	dre-miR-181c	2.0±0.1
13	*anxa2a*	Annexin A2a	2.6±0.7	0	–
14	*mpz*	Myelin protein zero	2.5±0.3	0	–
15	*zgc:64006*	Regulator of G protein signalling 5	2.5±0.3	dre-miR-19b	11.0±4.4
				dre-miR-19c	6.3±1.8
				dre-miR-181c	2.0±0.1
16	*slc25a4*	Solute carrier family 25 (mitochondrial carrier; adenine nucleotide translocator), member 4	2.5±0.3	dre-miR-181c	2.0±0.1
				dre-miR-199	2.8±0.4
17	*uqcrfs1*	Ubiquinol-cytochrome *c* reductase, Rieske iron-sulphur polypeptide 1	2.4±0.4	0	–
18	*zgc:109940*	Similar to complement factor D preparation	2.3±0.4	0	–
19	*wu:fc83c01*	Mitogen-activated protein kinase 4 isoform b	2.2±0.4	0	–
20	*necab1*	N-terminal EF-hand calcium binding protein 1	2.2±0.4	0	–
21	*tnk2*	Tyrosine kinase, non-receptor 2	2.2±0.4	0	–
22	*eno3*	Enolase 3 (β, muscle)	2.2±0.2	NI	–
23	*ndpkz2*	Nucleoside diphosphate kinase-22	2.2±0.2	NI	–
24	*rtna*	Reticulon 4a isoform 4-l	2.1±0.2	0	–
25	*mdhlb*	Malate dehydrogenase 1b, NAD (soluble)	2.1±0.2	0	–
26	*arl6ip1*	ADP-ribosylation factor-like 6 interacting protein 1	2.0±0.2	dre-miR-130b	8.3±1.6
				dre-miR-130c	1.9±0.3
27	*zgc:153978*	Orthologue of cytochrome *c* oxidase subunit 5B	2.0±0.2	0	–
28	*zgc:86773*	Ras-related protein Rab-1B	2.0±0.1	dre-miR-218b	2.9±0.3
29	*mfsd2b*	Major facilitator superfamily domain containing 2b	2.0±0.1	0	–
30	*scinla*	Scinderin-like A	2.0±0.2	0	–

Predicted target matches with down-regulated miRNAs at the $P<0.05$ level from miRBase Targets version 5 are shown (http://microrna.sanger.ac.uk/targets/v5/).
NI, no information available on miRBase.

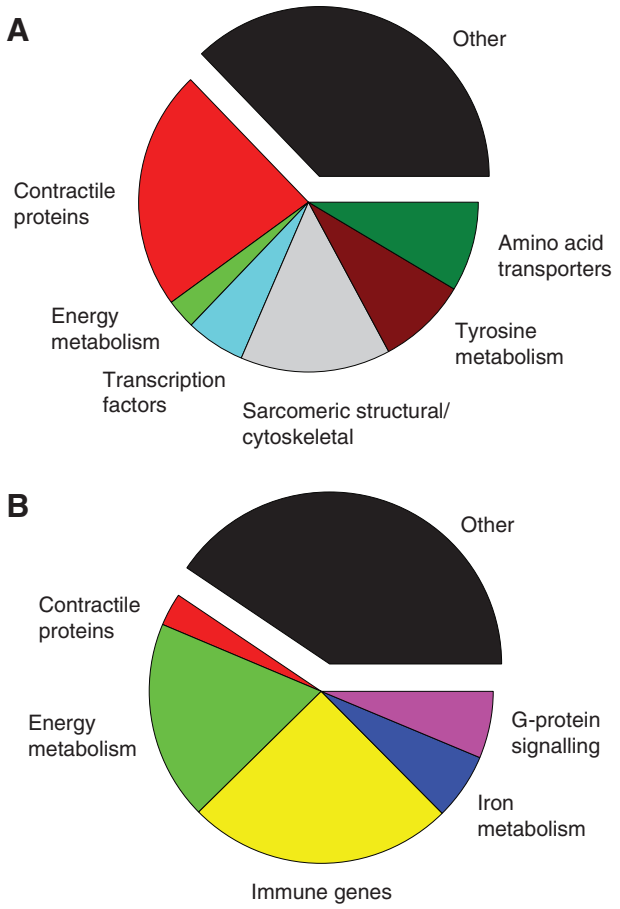

Fig. 5. Categorisation of (A) down- and (B) up-regulated mRNA transcripts in the M^- phenotype of adult zebrafish fast myotomal muscle.

production throughout the myotome (mosaic hyperplasia) (Rowlerson and Veggetti, 2001). Mosaic hyperplasia is absent in some fish species that only attain a small ultimate body length, e.g. the guppy (*Poecilia reticulata*) (Veggetti et al., 1993). It has been reported in the literature that mosaic hyperplasia is also absent in zebrafish restricting its use as a general model for teleost post-embryonic myogenesis (see Biga and Goetz, 2006), although this study examined only relatively small fish. Recently mosaic hyperplasia was observed in zebrafish larva at 6 mm standard length (~7.5 mm TL) (Patterson et al., 2008). The present study considerably extends these observations and demonstrates that mosaic hyperplasia is the main mechanism of muscle fibre expansion in zebrafish, as is the case for larger fish of commercial importance such as Atlantic salmon (*Salmo salar* L.) (see Johnston, 2006). This is an important finding because, compared with most farmed species, zebrafish has considerable advantages for investigation of the genetic mechanisms controlling growth, including the impact of selection and domestication. For example, in addition to a sequenced genome (http://www.ensembl.org/Danio_rerio/index.html) the small size and short generation time (~4 months) of zebrafish are ideal for maintaining replicated selected and non-selected lines at relatively low cost.

Zebrafish is a good model for investigating developmental plasticity of myogenesis

Embryonic temperature has been shown to alter the number and diameter of fast and slow myotomal muscle fibres in a phylogentically diverse range of teleost species (reviewed by Johnston, 2006). However, only a few studies have determined the long-term consequences of embryonic temperature for muscle growth in adult stages (Johnston et al., 2003; Macqueen et al., 2008; López-Albors et al., 2008). Macqueen and colleagues (Macqueen et al., 2008) incubated Atlantic salmon embryos at 2, 5, 8 or 10°C until the completion of eye pigmentation and then transferred them to common rearing conditions. Fish at lower temperatures remained smaller until smoltification 18 months later, but showed substantial compensatory catch-up growth in seawater over the next 18 months. The final number of fast muscle fibres was highest for the 5°C treatment and reduced at higher and lower treatments (Macqueen et al., 2008). ET treatment was also shown to alter the number of myonuclei per centimetre of fibre length in isolated single muscle fibres in this species (Johnston et al., 2003). In the present study, we found that zebrafish showed an optimal embryonic temperature for FFN of 26°C, which resulted in 18.8% more fast fibres than at 22°C and 13.7% more fibres than at 31°C (Table 1). Therefore zebrafish provides a good model for developmental plasticity to temperature in commercial species such as Atlantic salmon (Fig. 1), but has the advantage that the outcome of embryonic treatment on FFN can be established in less than 3 months. The present study showed that embryonic temperature affects both the intensity of myotube production (Fig. 1) and the body length at which the transition between M^+ and M^- phenotypes is completed and the FFN established (Table 1), extending previous studies. These observations require direct temperature effects on embryonic tissues such as the myogenic stem cell containing external cell layer. Cell lineage and vital dye tracking studies in zebrafish have shown that during mid-segmentation the somites undergo a 90 deg. rotation from their starting positions (Hollway et al., 2007). The cells in the posterior somite domain differentiate into the primary embryonic fast muscle fibres whereas those in the anterior compartment form the external cell layer on the outside of the embryonic slow muscle layer (Hollway et al., 2007; Stellabotte et al., 2007). Cells derived from the Pax3/7-expressing external cells migrate through the somite to form additional fast muscle fibres in the late embryo and larval stages (Hollway et al., 2007; Stellabotte et al., 2007). As the external cell layer persists in later stages it is a strong candidate for providing some or all of the myogenic progenitor cells required for juvenile and adult growth (Hollway et al., 2007; Stellabotte et al., 2007). We next used microarrays to obtain genome-wide information on changes in miRNA and mRNA expression between the M^+ and M^- phenotypes.

Gene expression changes associated with the transition from hyperplastic (M^+) to hypertrophic (M^-) phenotypes

We have chosen to investigate changes in gene and regulatory RNA expression between two complex growth phenotypes delineated by the active production of myotubes in fast myotomal muscle. Growth involves a population(s) of myogenic progenitor cells (MPCs) or myoblasts that remain capable of proliferation and are regulated by signalling pathways responsive to both nutritional status and environmental conditions. Myoblast fusion involves several processes, including the recognition and adhesion of myoblasts, the breakdown of muscle membranes and the remodelling of the actin cytoskeleton (Richardson et al., 2008). The primary event in myotube formation is myoblast–myoblast fusion giving rise to a syncytial structure with several nuclei. The secondary events of myotube elongation involve the accretion of a large number of additional nuclei and appear to involve distinct myoblast–myotube fusion events and separate regulatory pathways (Horsley and

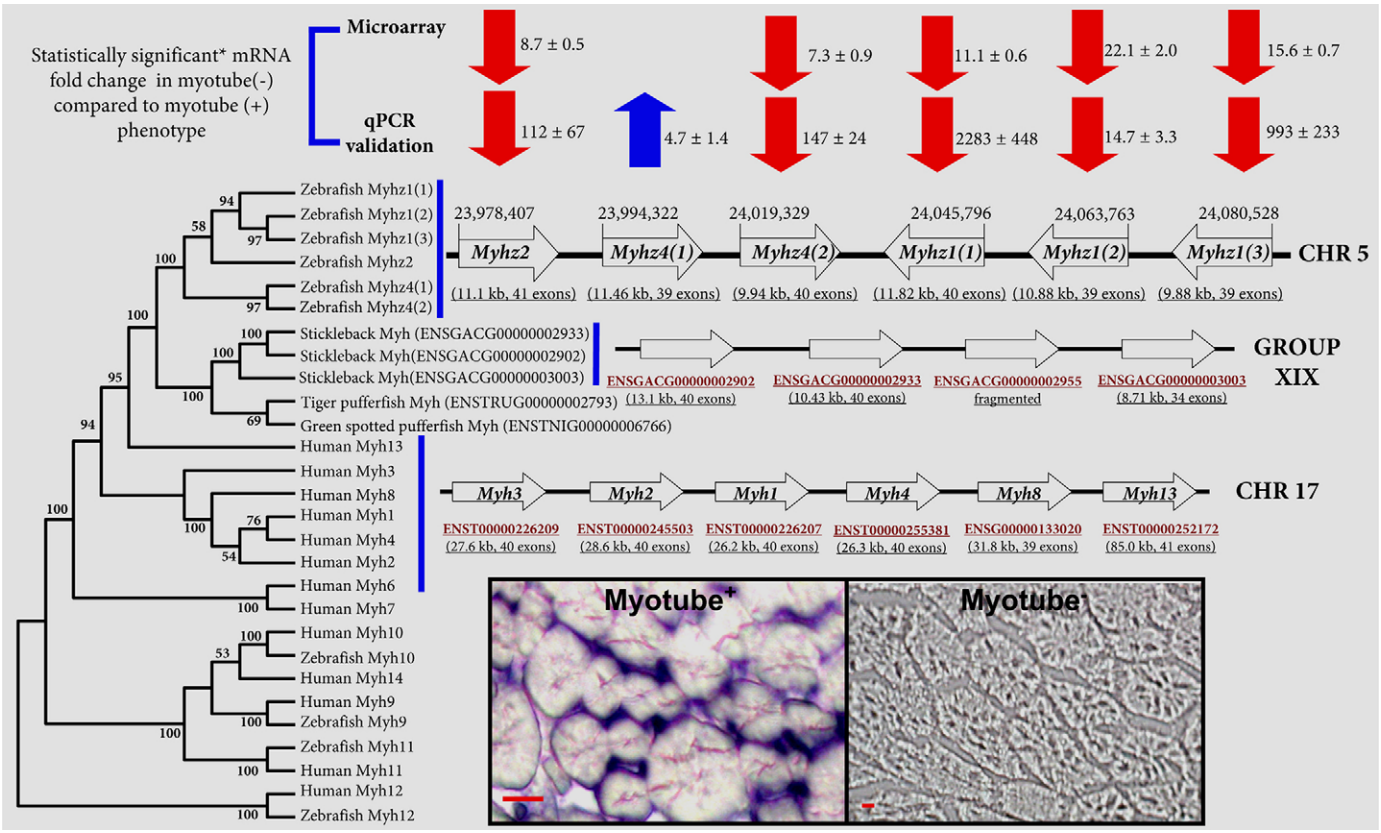

Fig. 6. The genomic organisation of a tandem of six fast skeletal myosin heavy chain (MyHC) genes found on chromosome 5 of zebrafish, five of which were highly differentially expressed between M^+ and M^- phenotypes. Details included about the genes are their total size, number of exons and position on chromosome 5. Shown above the cluster are fold difference values in mRNA expression levels from microarray and qPCR data (both obtained as discussed in text, also see Tables 2 and 4). Shown below the zebrafish tandem are similar clusters of fast skeletal MyHC genes found in sticklebacks and human genomes with details provided including Ensembl release 51 gene identifiers, gene size and number of exons. A maximum likelihood phylogenetic tree shown to the left of the diagram, as well as neighbour joining and maximum parsimony trees (not shown) suggested that these arrangements were independent, lineage-specific acquisitions (see main text). Shown at the bottom of the figure is the expression pattern of one of the zebrafish MyHC genes [*myhz1(2)*] in M^+ and M^- muscle fibre cross cryosections. The antisense probe was detected solely in small-diameter fibres in M^+ muscles and no signal was detected in either M^- or sense controls (not shown). The scale bar is 10 μm.

Pavlath, 2004). Genetic analysis involving *Drosophila* has identified a set of genes that have conserved functions in myotube formation across the metazoans (Richardson et al., 2008). Myoblast fusion and muscle formation were disrupted in zebrafish embryos lacking a functional *Rac* gene, which encodes a small GTPase that regulates the actin cytoskeleton (Pajinici et al., 2008). In mammals, two conserved orthologues of *Drosophila Bag2* and *Dock180* respectively activated the GTPases *AFR6* (ADP ribosylation factor 6) and *Rac* and were required for myoblast fusion and myotube differentiation (Pajcini et al., 2008). Knockdowns of *Dock1* and *Dock5* orthologues of the *Drosophila* gene myoblast city (*Mbc*) also result in the failure of myoblasts to fuse (Moore et al., 2007). Several genes and pathways have been discovered that are associated with the secondary events of myotube formation including the cytokine coding interleukin 4, IL-4 (Horseley et al., 2003) and myoferlin (Doherty et al., 2005). For example, the transcription factor NFATC2 regulates secretion of IL-4, which is essential for nuclear accretion during myotube elongation. Myoblasts derived from *NFATC2*$^{-/-}$ mice still form thin syncitial structures with a few nuclei associated with primary myotube formation, but fail to recruit additional nuclei and increase in diameter in the same way as cultures from wild-type animals (Horsley et al., 2003). In mammals another cytokine, interleukin-6 (IL-6), which is locally and transiently produced by growing myofibres and associated satellite cells is involved in muscle fibre hypertrophy (Serrano et al., 2008). There is evidence that IL-6 deficiency impairs myoblast proliferation and myonuclear accretion in growing muscle by impairing STAT3 activation and expression of its target gene *cyclin D1* (Serrano et al., 2008). It is therefore to be expected that myotube formation (specific to the M^+ phenotype) would share some common mechanisms and patterns of gene expression with muscle fibre growth involving fibre hypertrophy (present in the M^+ and M^- phenotypes) as well as having its own distinct features.

Genes associated with sarcomere structural proteins and the cytoskeleton comprised ~15% of the significantly down-regulated genes in the M^- phenotype (Fig. 5). Thymosin β4, the seventh most down-regulated gene in the M^- phenotype, is an actin monomer-sequestering protein regulating unpolymerised actin to control the assembly of microfilaments (Dedova et al., 2006), which has been implicated in promoting cell migration, angiogenesis, cell survival and wound healing. Studies with C2C12 myoblasts have shown that promyogenic members of the Ig superfamily bind to each other in a *cis* fashion, forming complexes with N- and M-cadherin. These complexes contain β-catenin and are enriched at sites of cell–cell

Table 4. Validation of microarray mRNA expression patterns using qPCR for 16 candidate genes

Gene	Relative expression level in M^- *versus* M^+ phenotype[a]	s.e.m.	*P*-value[b]
asporin	0.08	0.015	0.003
b2m	5.08	3.3	0.006
cd9l	2.42	1.7	0.007
hifan	4.2	2.7	0.007
myf5	0.49	0.2	0.16
myhz1(1)	0.000438	0.8 e–4	<0.0001
myhz1(2)	0.067	0.002	<0.0001
myhz1(3)	0.001	0.0002	<0.0001
myhz2	0.0009	0.004	0.001
myhz4(1)	4.69	1.4	0.04
myhz4(2)	0.007	0.001	<0.0001
myoz1	1.23	0.4	0.678
pvalb4	16.9	10.9	0.005
tnni2	0.33	0.16	0.01
tyrp1b	0.27	0.05	0.01
zgc:64006	7.1	1.36	0.03

All expression values were normalised to β-actin and *rpl13* housekeeping genes that were stably expressed between M^+ and M^- samples.

[a]The stated expression value is relative to a value of 1 for the M^- phenotype.

[b]*P*-value is from a randomisation test using 5000 bootstrap iterations testing the hypothesis that differences between M^+ and M^- samples is due solely to chance (reject hypothesis at $P<0.05$).

contact between myoblasts (Kang et al., 2003). In the M^- phenotype of zebrafish, *ctnna2*, an orthologue of human catenin, was down-regulated 2.2-fold (Table 2). Another of the down-regulated genes in the zebrafish M^- phenotype was *aspn*, which is one of the class I members of the small leucine-rich repeat proteoglycans (SLRPs) which also include decorin and biglycan (Henry et al., 2001). In the mouse, asporin is strongly expressed in the skeleton and more weakly in the fascia surrounding muscle fibres (Henry et al., 2001). Asporin inhibits TGF-B/Smad signalling by colocalising with TGFB-1 on the cell surface and inhibiting its binding to the TGFB type II receptor (Nakajima et al., 2007). Knockdown of asporin by small interfering RNA (siRNA) inhibits TGF-B1-induced gene expression and blocks chondrogenesis (Nakajima et al., 2007) whereas targeted mutations of class I SRLPs result in abnormal collagen fibril formation (Henry et al., 2001).

The second largest category of up-regulated genes in the M^- phenotype were immune-related genes, including several that function in cytokine pathways and are therefore candidates for involvement with myoblast fusion and/or muscle hypertrophy. Several transmembrane proteins containing immunoglobulin domains function in the recognition and adhesion of myoblasts (Richardson et al., 2008). The second most highly up-regulated gene in the M^- phenotype was *b2m* which functions in the folding, peptide binding and surface display of class I antigens (Yu et al., 2009). CD9 antigen-like (*cd9l*), which was down-regulated ~2.5 times (Tables 3 and 4), is a cell surface molecule that interacts with integrins and other membrane proteins. Most cytokine receptors are capable of recruiting and/or activating non-receptor protein kinases that induce downstream signalling pathways (Taniguchi, 1995). Tyrosine kinase, non-receptor 2 (*tnk2*) was up-regulated 2.2-fold in the M^- phenotype (Table 3). There is evidence that macrophages are involved in muscle regeneration and can stimulate myogenic cell growth *in vitro* promoting myoblast fusion into myotubes and myogenin expression leading to differentiation (Arnold et al., 2007). Invariant chain-like protein (CD74 antigen) has MHC2 interacting and thyroglobulin domains.

Our gene expression analysis has successfully identified five paralogues of fast skeletal myosin heavy chain organised in a tandem repeat on chromosome 5 of zebrafish that are very highly down-regulated in the M^- phenotype and specifically expressed in very small diameter muscle fibres (Fig. 6). Several of these genes are also highly expressed in the somites of zebrafish embryos (Xu et al., 2000). Myosin heavy chain isoforms specific to small diameter muscle fibres have previously been reported in the common carp (*Cyprinus carpio* L.) (Ennion et al., 1999). Interestingly, phylogenetic analysis suggests that these tandem copies and similar clusters of orthologous myosin heavy chain genes found in other vertebrates including stickleback and human (Fig. 6) as well as medaka (Liang et al., 2007) are not synapomorphies and were derived separately in each of these lineages. This suggests that some selective advantage exists, at least in some vertebrates, for having multiple tandem copies of MyHC genes. However, considering that one of the zebrafish tandem copies was not down-regulated in M^- zebrafish, it is possible that complex lineage-specific patterns of myosin heavy chain gene regulation has occurred, which might contribute to species-specific differences in fast-twitch myotube formation patterns.

Numerous aspects of muscle phenotype can be correlated with changes in body size. For example, the maximum tail-beat frequency (contraction duration per cycle) and aerobic metabolic capacity are known to decrease with increasing body length (James et al., 1998; Davies and Moyes, 2007). We found a huge fold increase in *pvalb4* expression in the M^- phenotype (Tables 3 and 4). Pvalb4 is a cytoplasmic Ca^{2+} binding protein involved in muscle relaxation. In the rainbow trout, the content of parvalbumin isoform 1 was shown to decrease along the trunk and was associated with a slowing of muscle relaxation rate (Coughlin et al., 2007), as occurs with increasing body size. An orthologue of the myozenin gene (*myoz1*; calsarcin–calcineurin binding protein) was down-regulated 2.3-fold in the M^- phenotype on the microarray (Table 2), although no significant difference in expression was observed by qPCR when independent M^+ and M^- samples were used (Table 4). *Myoz1* knockout mice are deficient in calsarcin-2 and show enhanced NFAT activity and calcineurin signalling leading to a slower oxidative phenotype (Frey et al., 2008). The higher mRNA levels of *myoz1* observed in the M^+ phenotype on the array may be related to the increased aerobic character of fast muscle observed in small compared with large fish (Davies and Moyes, 2007).

Role of miRNAs in the transition between muscle growth phenotypes

Fourteen up-regulated (Fig. 2) and 15 down-regulated miRNAs (Fig. 3) were identified in the M^- phenotype providing evidence for the involvement of miRNAs in muscle growth transitions; 57% of the down-regulated mRNAs and 73% of the up-regulated mRNAs were predicted targets for one or more differentially expressed miRNAs (Figs 2 and 3; Tables 2 and 3). Bioinformatic approaches to identify mRNA targets for miRNAs have involved assessing Watson–Crick base-pairing at nucleotides 2–7 at the 5′ end of the miRNA (the so-called 'seed match') (Brennecke et al., 2005). However, many computationally predicted targets have failed to be confirmed experimentally (Didiano and Hobert, 2006) and some validated miRNAs were not identified by the current algorithms (Nicolas et al., 2008). miRNA target site interactions may also involve local accessibility of the binding site. Validated miRNA target sites often have destabilising elements or high free energy in regions flanking the 5′ or 3′ ends of the target site (Xiao et al., 2009). The popular computational miRNA–mRNA prediction algorithm miRanda detects potential target sites based on the alignment score and minimum free energy (MFE) of the miRNA bound to the potential target site, and is likely to overestimate the number of true targets (Moxon et al., 2008). Thus the strongest candidate miRNAs to have a role in this growth transition are those with multiple targets. Of particular interest was dre-miR-181c which was expressed at a 2-fold lower level in the M^- phenotype and was predicted to bind to the 3′ UTR of five of the up-regulated genes *pvalb4*, *gapdh*, *cd9l*, *zgc:64006* and *slc25a4* (Table 3). It is of interest that miR-181 has been shown to be up-regulated before or at the same time as muscle differentiation markers such as creatine kinase in cell culture (Naguibeva et al., 2006). *In vivo* miR-181 was weakly expressed in adult mouse tibial muscle, but was strongly up-regulated following repair from injury (Naguibeva et al., 2006). miR-181 was also shown to repress the translation of Hox-A11 a repressor of the differentiation program (Naguibeva et al., 2006).

MiR-1 and miR-206 are known from functional and expression studies to interact with conserved transcriptional networks regulating myogenesis (Callas et al., 2008) and were significantly differentially expressed between phenotypes, but at less than 2-fold (not shown). For example, miR-206 was 31% higher in the M^+ phenotype, which contained actively differentiating muscle fibres, whereas miR-133c expression was not significantly different between phenotypes. These two miRNAs have been shown to be induced by transferring C2C12 myoblasts to differentiation medium (Kim et al., 2006). Although miR-206 transfection advanced myosin heavy chain expression after changing to differentiation medium, miR-133 transfection did not. Inhibition of miR-206 by antisense oligonucleotide inhibited cell cycle withdrawal and differentiation and evidence was presented that mRNA for the p180 subunit of DNA polymerase was degraded by miR-206 (Kim et al., 2006). miR-206 also regulates the expression of connexin43, a component of gap junctions required for the fusion of myoblasts and muscle differentiation *in vitro* (Anderson et al., 2006). However, in this case regulation occurs by inhibiting translation without targeting the mRNA for degradation (Anderson et al., 2006).

This research was supported by a consortium grant (NE/C508077/1) from the Natural Environment Research Council of the UK. We are grateful to Ian Amaral and Vera Vieira-Johnston for their invaluable assistance with zebrafish husbandry and to Dr Charles Paxton, School of Mathematics for his help with statistical analyses.

REFERENCES

Anderson, C., Catoe, H. and Werner, R. (2006). MIR-206 regulates connexin43 expression during skeletal muscle development. *Nucleic Acids Res.* **34**, 5863-5871.
Arnold, L., Henry, A., Poron, F., Baba-Amer, Y., van Rooijen, N., Plonquet, A., Gherardi, R. K. and Chazaud, B. (2007). Inflammatory monocytes recruited after skeletal muscle injury switch into anti-inflammatory macrophages to support myogenesis. *J. Exp. Med.* **204**, 1057-1069.
Bagga, S., Brach, J., Hunter, S., Massirer, K., Holtz, J., Eachus, R. and Pasquinelli, A. E. (2005). Regulation by let-7 and line 4 miRNAs result in target mRNA degradation. *Cell* **122**, 553-563.
Bartel, D. P. (2004). MicroRNAs: genomics, biogenesis, mechanisms and function. *Cell* **116**, 281-297.
Biga, P. R. and Goetz, F. W. (2006). Zebrafish and giant Danio as models for muscle growth: determinate vs indeterminate growth as determined by morphometric analysis. *Am. J. Physiol. Regul. Integr. Comp. Physiol.* **291**, R1327-R1337.
Brennecke, J., Stark, A., Russell, R. B. and Cohen, S. M. (2005). Principles of microRNA-target recognition. *PloS Biol.* **3**, e85.
Callas, T. E., Deng, Z., Chen, J. F. and Wang, D. W. (2008). Muscling through the microRNA world. *Exp. Biol. Med.* **233**, 131-138.
Chan, S. P. and Slack, J. J. (2006). MicroRNA silencing inside P-bodies *RNA Biol.* **3**, 97-100.
Chen, J. F., Mandel, E. M., Thomson, J. M., Wu, Q., Callis, T. E., Hammond, S. M., Coplon, F. L. and Wana, D. Z. (2006). The role of micro RWA-T and microRNA-133 in skeletal muscle proliferation and differentiation. *Nat. Genet.* **38**, 228-233.
Coughlin, D. J., Solomon, S. and Wilwert, J. L. (2007). Parvalbumin expression in trout swimming muscle correlates with relaxation rate. *Comp. Biochem. Physiol. A* **147**, 1074-1082.
Davies, R. and Moyes, C. D. (2007). Allometric scaling in centrarchid fish: origins of intra- and inter-specific variation in oxidative and glycolytic enzyme levels in muscle. *J. Exp. Biol.* **210**, 3798-3804.
Dedova, I. V., Nikolaeva, O. P., Safer, D., De La Cruz, E. M. and dos Remedios, C. G. (2006). Thymosin beta(4) induces a conformational change in actin monomers. *Biophys. J.* **90**, 985-992.
Didiano, D. and Hobert, O. (2006). Perfect seed pairing is not a generally reliable predictor for miRNA-target interactions. *Nat. Struct. Mol. Biol.* **13**, 849-851.
Doench, J. G. and Sharp, P. A. (2004). Specificity of microRNA target selection in translational repression. *Genes Dev.* **18**, 504-511.
Doherty, K. R., Cave, A., Davis, D. B., Delmonte, A. J., Posey, A., Earley, J. U., Hadhazy, M. and McNally, E. M. (2005). Normal myoblast fusion requires myoferlin. *Development* **24**, 5565-5575.
Ennion, S., Wiles, D., Gauvry, L., Alami-Durante, H. and Goldspink, G. (1999). Identification and expression analysis of two developmentally regulated myosin heavy chain gene transcripts in carp (*Cyprinus carpio*). *J. Exp. Biol.* **202**, 1081-1090.
Fernandes, J. M. O., Mackenzie, M. G., Elgar, G., Suzuki, Y., Watabe, S., Kinghorn, J. R. and Johnston, I. A. (2005). A genomic approach to reveal novel genes associated with myotube formation in the model teleost, *Takifugu rubripes*. *Physiol. Genomics* **22**, 327-338.
Frey, N., Frank, D., Lippi, S., Kuhn, C., Kögler, H., Barrientos, T., Rohr, C., Will, R., Müller, O. J., Weiler, H. et al. (2008). Calsarcin-2 deficiency increases exercise capacity in mice through calcineurin/NAFT activation. *J. Clin. Invest.* **118**, 3598-3608.
Guindon, S. and Gascuel, O. (2003). A simple, fast, and accurate algorithm to estimate large phylogenies by maximum likelihood. *Syst. Biol.* **52**, 696-704.
Henry, S. P., Takanosu, M., Boyd, T. C., Mayne, P. M., Eberspaecher, H., Zhou, W., de Crombrugghe, B. and Mayne, M. (2001). Expression pattern and gene characterization of asporin: a newly discovered member of the leucine-rich repeat protein family. *J. Biol. Chem.* **276**, 12212-12221.
Hollway, G. E., Bryson-Richardson, R. J., Berger, S., Cole, N. J., Hall, T. E. and Currie, P. D. (2007). Whole-somite rotation generates muscle progenitor cell compartments in the developing zebrafish embryo. *Dev. Cell* **12**, 207-219.
Horsley, V. and Pavlath, G. K. (2004). Forming a multinucleated cell: molecules that regulate myoblast fusion. *Cells Tissues Organs* **176**, 67-78.
Horsley, V., Jansen, K. M., Mills, S. T. and Pavlath, G. K. (2003). IL-4 acts as a myoblast recruitment factor during mammalian muscle growth. *Cell* **113**, 483-494.
Hutvagner, G. and Zanmore, P. D. (2002). A microRNA in a multiple-turnover RNA: enzyme complex. *Science* **297**, 2056-2060.
James, R. S., Cole, N. J., Davies, M. L. F. and Johnston, I. A. (1998). Scaling of intrinsic contractile properties and myofibrillar protein composition of fast muscle fibres in the short-horn sculpin (*Myoxocephalus scorpius*). *J. Exp. Biol.* **201**, 901-912.
Jiang, Y., Johnson, J. D. and Rall, J. A. (1996). Parvalbumin relaxes frog skeletal muscle when sarcoplasmic reticulum Ca^{2+}-ATPase is inhibited. *Am. J. Physiol. Cell Physiol.* **39**, C411-C417.
Johnston, I. A. (2006). Environment and plasticity of myogenesis in teleost fish. *J. Exp. Biol.* **209**, 2249-2264.
Johnston, I. A., Strugnell, G., McCracken, M. C. and Johnstone, R. (1999). Muscle growth and development in normal-sex ratio and all-female diploid and triploid Atlantic salmon. *J. Exp. Biol.* **202**, 1991-2016.
Johnston, I. A., Manthri, S., Alderson, R., Smart, A., Campbell, P., Nickell, D., Robertson, B., Paxton, C. G. M. and Burt, M. L. (2003). Freshwater environment affects growth rate and muscle fibre recruitment in seawater stages of Atlantic salmon (*Salmo salar*). *J. Exp. Biol.* **206**, 1337-1351.
Johnston, I. A., Abercromby, M., Vieira, V. L. A., Sigursteindóttir, R. J., Kristjánsson, B., Sibthorpe, D. and Skúlason, S. (2004). Rapid evolution of muscle fibre number in post-glacial populations of Arctic charr *Salvelinus alpinus*. *J. Exp. Biol.* **207**, 4343-4360.
Kang, J.-S., Feinleib, J. L., Knox, S., Ketteringham, M. A. and Krauss, R. S. (2003). Promyogenic members of the Ig and cadherin families associate to positively regulate differentiation. *Proc. Natl. Acad. Sci. USA* **100**, 3984-3994.
Kim, H. K., Lee, Y. S., Sivaprad, U., Malhotra, A. and Dulta, A. (2006). Muscle-specific microRNA miR-206 promotes muscle differentiation. *J. Cell Biol.* **174**, 677-687.

Kiriakidou, M., Tan, G. S., Lamprinaki, S., De Planell Sauger, M., Nelson, P. T. and Monrelatos, Z. (2007). An mRNA m7G cap binding-like motif within human Ago2 represses translation. *Cell* **129**, 1141-1151.

Lee, Y., Ahn, C., Han, J., Choi, H., Kim, J., Yim, J., Lee, J., Provost, P., Radmark, O., Kim, S. et al. (2003). The nuclear Rnase III Drosha initiates microRNA processing. *Nature* **425**, 415-419.

Lewis, B. P., Burge, C. B. and Bartel, D. P. (2005). Conserved seed pairing often flanked by adenosines, indicates that thousands of human genes are microRNA targets. *Cell* **120**, 15-20.

Liang, C. S., Kobiyama, A., Shimizu, A., Sasaki, T., Asakawa, S., Shimizu, N. and Watabe, S. (2007). Fast skeletal muscle myosin heavy chain gene cluster of Medaka *Oryzias latipes* enrolled in temperature adaptation. *Physiol. Genomics* **29**, 201-214.

López-Albors, O., Abdel, I., Periago, M. J., Ayala, M. D., Alcázar, A. G., Graciá, C. M., Nathanailides, C. and Vázquez, J. M. (2008). Temperature influence on the white muscle growth dynamics of the sea bass *Dicentrarchus labrax* L. Flesh quality implications at commercial size. *Aquaculture* **277**, 39-51.

Lu, J., McKinsey, T. A., Zhana, C. L. and Olson, E. N. (2000). Regislation of skeletal myogenesis by association of the MEF2 transcription factor with class II histone deacetylases. *Mol. Cell* **6**, 233-244.

Macqueen, D. J., Robb, D. H. F., Olsen, T., Melstveit, L., Paxton, C. G. M. and Johnston, I. A. (2008). Temperature until the 'eyed stage' of embryogenesis programmes the growth trajectory and muscle phenotype of adult Atlantic salmon. *Biol. Lett.* **4**, 294-298.

McCarthy, J. J and Esser, K. A. (2007). MicroRNA-1 and microRNA-133, expression are decreased during skeletal muscle hypertrophy. *J. Appl. Physiol.* **102**, 306-313.

Moore, C. A., Parkin, C. A., Bidet, Y. and Ingham, P. W. (2007). A role for the myoblast city homologues Dock1 and Dock5 and the adaptor proteins Crk and Crk-like in zebrafish myoblast fusion. *Development* **134**, 3145-3153.

Moxon, S., Moulton, V. and Kim, J. T. (2008). A scoring matrix approach to detecting miRNA target sites. *Algorithms Mol. Biol.* 2008. 3:3.

Naguibneva, L., Ameyar-Zazoua, M., Polesskaya, A., Ait-Si-Ali, S., Groisman, R., Souidi, M., Cuvellier, S. and Harel-Bellan, A. (2006). The microRNA miR-181 targets the homeobox protein Hox: all during mammalian myoblast differentiation. *Nat. Cell Biol.* **8**, 278-284.

Nakajima, M., Kizawa, H., Saitoh, M., Kou, I., Miyazono, K. and Ikegawa, S. (2007). Mechanisms for asporin function and regulation in articular cartilage. *J. Biol. Chem.* **282**, 32185-32192..

Nicolas, F. E., Pais, H., Schwach, F., Lindow, M., Kauppinen, S., Moulton, V. and Dalmay, T. (2008). Experimental identification of microRNA-140 targets by silencing and overexpressing miR-140. *RNA* **14**, 2513-2520.

Okamura, K., Phillips, M. D., Tyler, D. M., Duan, H., Chou, Y. T. and Lai, C. (2008). The regulatory activity of microRNA* species has substantial influence on microRNA and 3′UTR evolution. *Nature Struct. Mol. Biol.* **15**, 354-363.

Pajcini, K. V., Pomerantz, J. H., Alkan, O., Doyonnas, R. and Blau, H. M. (2008). Myoblasts and macrophages share molecular components that contribute to cell-cell fusion. *J. Cell Biol.* **180**, 1005-1019.

Patterson, S. E., Mook, L. B. and Devoto, S. H. (2008). Growth in the larval zebrafish pectoral fin and trunk musculature. *Dev. Dyn.* **237**, 307-315.

Pei, J. and Grishin, N. V. (2007). PROMALS: towards accurate multiple sequence alignments of distantly related proteins. *Bioinformatics* **23**, 802-808.

Pfaffl, M. W., Horgan, G. W. and Dempfle, L. (2002). Relative expression software tool (REST) for group-wise comparison and statistical analysis of relative expression results in real-time PCR. *Nucleic Acids Res.* **30**, e36.

Pinheiro, J. C. and Bates, D. M. (2000). *Mixed-effects Models in S. and S-plis*. New York: Springer.

Rao, P. K., Kumar, P. M., Farkhondeth, M., Baskerville, S. and Lodish, H. F. (2006). Myogenic factors that regulate the expression of muscle-specific micro RNAs. *Proc. Natl. Acad. Sci. USA* **103**, 8721-8726.

Richardson, B. E., Nowak, S. J. and Baylies, M. K. (2008). Myoblast fusion in fly and vertebrates: new genes, new processes and new perspectives. *Traffic* **9**, 1050-1059.

Rosenberg, M. I., Georges, S. A., Asawachaicharm, A., Analau, E. and Tapscott, S. J. (2006). MyoD inhibits Fst 1and Utrn expression by inducing transcription of miR-206. *J. Cell Biol.* **175**, 77-85.

Rowlerson, A. and Veggetti, A. (2001). Cellular mechanisms of post-embryonic muscle growth in aquaculture species. In *Fish Physiology 18: Muscle Development and Growth* (ed. I. A. Johnston), pp. 103-140. New York: Academic Press.

Semenza, G. L. (1999). Regulation of mammalian O_2 homeostasis by hypoxia-inducible factor 1. *Annu. Rev. Cell Dev. Biol.* **15**, 551-578.

Serrano, A. L., Baeza-Raja, B., Perdiguero, E., Jardi, M. and Muñoz-Cánoves, P. (2008). Interleukin-6 is an essential regulator of satellite cell-mediated skeletal muscle hypertrophy. *Cell Metab.* **7**, 33-44.

Stellabotte, F., Dobbs-McAuliffe, B., Fernandez, D. A., Feng, X. and Devoto, S. H. (2007). Dynamic somite cell arrangements lead to distinct waves of myotomal growth. *Development* **134**, 1253-1257.

Sweetman, D., Goljanek, K., Rathjen, T., Oustanina, S., Braun, T., Dalmay, T. and Munsterberg, A. (2008). Specific requirements of MRFs for the expression of muscle specific microRNAs, miR-1, miR-206 and miR-133. *Dev. Biol.* **321**, 491-499.

Tamura, K., Dudley, J., Nei, M. and Kumar, S. (2007). MEGA4: molecular evolutionary genetics analysis (MEGA) software version 4.0. *Mol. Biol. Evol.* **24**, 1596-1599.

Taniguchi, T. (1995). Cytokine signaling through nonreceptor protein tyrosine kinases. *Science* **268**, 251-255.

Thisse, C. and Thisse, B. (2008). High-resolution *in situ* hybridization to whole-mount zebrafish embryos. *Nat. Protoc.* **3**, 59-69.

Tian, Z., Greene, A. S., Pietrusz, J. L., Matus, I. R. and Liang, M. (2008). MicroRNA-target pairs in the rat kidney identified by microRNA microarray, proteomic and bioinformatics analysis. *Genome Res.* **18**, 404-411.

Veggetti, A., Mascarello, F., Scapolo, P. A., Rowlerson, A. and Candia-Carnevali, M. D. (1993). Muscle growth and myosin isoform transitions during development of a small teleost fish, *Poecilia reticulata* (Peters) (Atheriniformes, Poeciliidae): a histochemical, immunohistochemical, ultrastructural and morphometric study. *Anat. Embryol.* **187**, 353-361.

Weatherley, A. H., Gill, H. S. and Lobo, A. F. (1988). Recruitment and maximal diameter of axial muscle fibres in teleosts and their relationship to somatic growth and ultimate size. *J. Fish Biol.* **33**, 851-859.

Williams, A. E. (2008). Functional aspects of animal MicroRNAs. *Cell. Mol. Life Sci.* **65**, 545-562.

Xiao, F. F., Zuo, Z. X., Cai, G. S., Kang, S. L., Gao, X. L. and Li, T. B. (2009). MiRecords: an integrated resource for microRNA-target interactions. *Nucleic Acids Res.* **37**, D105-D110.

Xu, Y., He, J., Wang, X., Lim, T. M. and Gong, Z. (2000). Asynchronous activation of 10 muscle-specific protein (MSP) genes during zebrafish somitogenesis. *Dev. Dyn.* **219**, 201-215.

Yang, G. D., Wu, L. Y., Jiang, B., Yang, W., Qi, J. S., Cao, K., Meng, Q. H., Mustafa, A. K., Mu, W. T., Zhang, S. M. et al. (2008). H_2S as a physiological vasorelaxant: hypertension in mice with deletion of cystathionine gamma-lyase. *Science* **322**, 587-590.

Yu, S., Chen, X. and Ao, J. (2009). Molecular characterization and expression analysis of beta(2)-microglobulin in large yellow croaker *Pseudosciaena crocea*. *Mol. Biol. Rep.* doi:10/1007/s11033-008-9373-6.

Zhao, Y. and Srivastava, D. (2007). A developmental view of microRNA function. *Trends Biochem. Sci.* **32**, 189-197.

Zhao, Y., Ransom, J. F., Li, A., Vedantham, V., von Drehle, M., Muth, A. N., Tsuchihashi, T., McManus, M. T., Schwartz, R. J. and Srivastava, D. (2007). Dysregulation of cardiogenesis, cardiac conduction and cell cycle in mice lacking miRNA-1-2. *Cell* **129**, 303-317.